Electrochemical Cells

DOI: 10.1002/ange.200803981

A Multiple Working Electrode for Electrochemical Cells: A Tool for Current Density Distribution Studies**

*See-How Ng, Fabio La Mantia, and Petr Novák**

In view of the ever-increasing crude-oil price, the need for alternative energy sources and storage for transportation is inevitable. Currently the technology of choice for future hybrid electric vehicles (HEVs) is the rechargeable lithium-ion battery, which has the capability to store 2–3 times more energy per unit mass and volume than the nickel-metal hydride battery.[1–3] One of the requirements for the mass production of lithium-ion batteries for use in HEVs is to increase the rate capability of the electrode materials.[4–5] However, the rate capabilities of both negative and positive electrode materials are low owing to the non-uniformity of current density distribution across the porous electrodes.[6–7] Therefore, it is important to understand the degree of the non-uniformity of the current density distribution across the porous electrode systems perpendicular to the current collector.

The theoretical background of current density distribution in porous electrodes has been developed over the past 50 years. There are two classes of models: the single-phase, and the two-phase model. In 1948, the first model of a porous electrode was developed by Daniel-Bekh,[8] which is a two-phase model, in which the liquid electrolyte and the solid electrode are treated as separate phases and the pores have a well-defined geometry. In 1960, Euler and Nonnenmacher[9] described the porous electrode as a single homogeneous phase consisting of a liquid electrolyte and a solid electrode. This single-phase model considered the current to be generated in the volume of the porous electrode. Euler and Nonnenmacher also simulated the current density distribution along the porous electrode by neglecting diffusion of the reactants and the products. In 1962, Newman and Tobias[10] introduced the effect of diffusion along the x axis and the dependence of the polarization resistance on the current distribution density in the single-phase model.[9] The transmission line model (TLM), developed by de Levie in the 1960's,[11–13] is based on the two-phase model of Daniel-Bekh, and considers only the radial diffusion of reactants and products. Most research on the specific current distribution in the lithium-ion battery system performed to date has been focused on theoretical modeling or dynamic simulation.[14–18] Herein, we report a multiple-working-electrode (MWE) electrochemical cell (Figure 1) with the capability to quantitatively measure the current density distribution across the electrode thickness, where inhomogeneity in current density distribution occurs owing to the different electrochemical overpotentials across the electrode. This difference in the electrochemical overpotential arises because of the thickness of the electrodes in which a concentration gradient is developed. To our knowledge, this is the first time in the

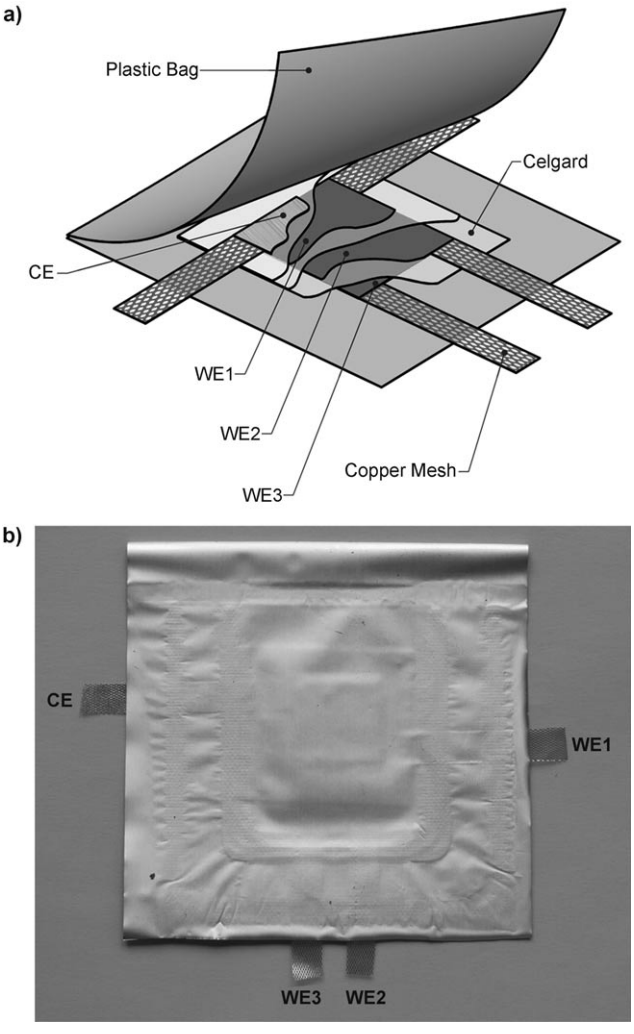

Figure 1. a) Sketch of the MWE electrochemical cell. b) Photo of an actual MWE electrochemical cell ($10\times10\,cm^2$) after sealing under vacuum. CE = counter electrode, WE = working electrode (the numbers indicate the position of the WE; the smaller the number, the closer the electrode is to the CE).

[*] Dr. S.-H. Ng, Dr. F. La Mantia, Priv.-Doz. Dr. P. Novák
Electrochemistry Laboratory, Paul Scherrer Institut
5232 Villigen PSI (Switzerland)
Fax: (+41) 56-310-4415
E-mail: petr.novak@psi.ch
Homepage: http://ecl.web.psi.ch/lithium

[**] Financial support by the Swiss National Science Foundation is gratefully acknowledged. Technical assistance from W. Scheifele, H. Kaiser, and Dr. F. Rosciano is highly appreciated. Finally, we would like to thank TIMCAL SA for providing the SFG44 graphite samples for this study.

InterScience DISCOVER SOMETHING GREAT
© 2009 Wiley-VCH Verlag GmbH & Co. KGaA, Weinheim

field of lithium-ion batteries an actual experimental result is obtained that directly measures the current density distribution perpendicular to the current collector.

Figure 1a shows the working electrodes (WEs) that are separated by a layer of an electrolyte-soaked polymeric separator, which acts as an ion conductor for the electrolyte solution and avoids electrical short-circuit among the WEs. This is a crucial point, as short-circuit between the WEs would mislead the current density distribution measurements. Another important feature of this MWE electrochemical cell is that the cell is vacuum-sealed under an argon atmosphere, which prevents moisture in the atmosphere to be in contact with the cell components. The final configuration of the MWE electrochemical cell is shown in Figure 1b. The geometry of the MWE electrochemical cell is not the classical geometry with porous electrodes. The current collector does not contact with the bottom of a porous electrode, but is a mesh incorporated in the electroactive material. Owing to the geometry of this electrochemical cell, the processes occurring in electrodes can be represented by the equivalent circuit given in Figure 2.

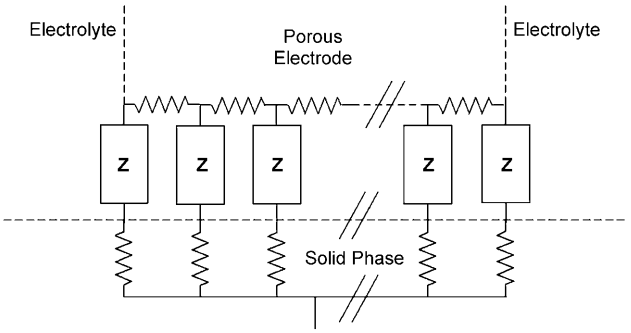

Figure 2. Equivalent-circuit representation of a porous electrode. Z represents the electrochemical processes.

The geometry of the MWE electrochemical cell is designed such that the specific resistance of the solid phase is independent of the position in the electrode; however, the non-uniformity of the current density distribution results from the different electrolyte concentrations in the liquid phase present in the pores of the electrodes. A mathematical description of the system applied in this study is given by Equations (1) and (2):

$$\frac{\partial^2 \Delta\phi}{\partial x^2} = \frac{r_s}{a}\left[C_{dl}\frac{\partial^2 \Delta\phi}{\partial t} + i_F(\Delta\phi, C_i)\right] \quad (1)$$

$$\frac{\partial^2 C_i}{\partial x^2} = \tau_{D,i}\left[\frac{\partial C_i}{\partial t} \pm \frac{i_F(\Delta\phi, C_i)}{a\, z\, F}\right] \quad (2)$$

where, $\Delta\phi$ is the potential drop across the interphase, r_S is the resistivity of the electrolyte solution, a is the parameter depending on the dimension of the pores, C_{dl} is the double-layer capacitance at the solid/electrolyte interphase, i_F is the Faradaic current, C_i is the concentration of species i, $\tau_{D,i}$ is the time constant of diffusion for species i, z is the number of electrons exchanged during the reaction, F is the Faraday constant. The plus sign (+) is used if species i is in the oxidized form and the minus sign (−) is used if species i is in the reduced form. From Equations (1) and (2), it is clear that differences in behavior during the charging/discharging for the three layers in the MWE electrochemical cell are due to the three main factors: r_S, $\tau_{D,I}$, and i_F.

Proper electrical connections between the WEs for this study are of utmost importance, as the main objective of this study is to quantify the specific current for each WE; but to suppress the mutual influence of those electrodes. To achieve this objective, we applied three additional potentiostats (P1, P2, and P3) for direct measurement of the respective specific current that passes into each layer of the WEs (Figure 3). The

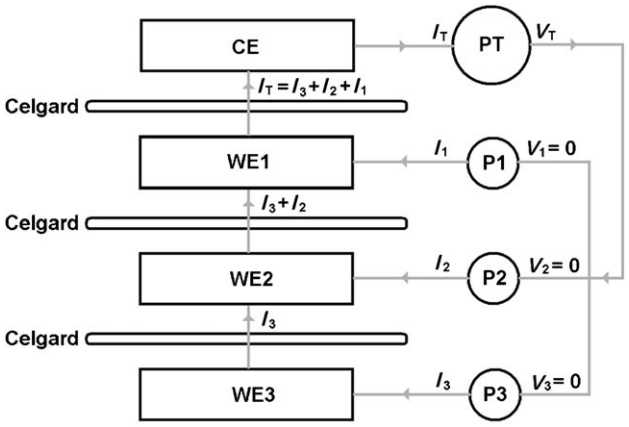

Figure 3. The electrical circuit applied in this study. CE = counter electrode, WE = working electrode (the numbers indicate the position of the WE; the smaller the number, the closer the electrode is to the CE), P = potentiostat, V = potential difference between the poles of the potentiostat, I = current measured, I_T = total current applied.

role played by each of these potentiostats in this case can be viewed as a "current follower",[19] which is a device that measures current without inducing a potential drop. In other words, the current is transferred without a potential drop through the potentiostat. Note that the distance between each of the WEs is assumed to be approximately the thickness of each polymeric separator, which is circa 25 μm with 55% porosity.

Galvanostatic cycling was performed on the MWE electrochemical cell depicted in Figure 1 using the electrical connections shown in Figure 3. Graphite was chosen as the model negative working electrode material because documenting non-uniform current density distribution in graphite electrodes is scientifically challenging.[1,6,7,20] Furthermore, the color change in the graphite electrodes can provide additional evidence for the non-uniformity in current density distribution.[20] To demonstrate these phenomena without a noticeable influence of other electrochemical cycling parameters, the galvanostatic measurements (Figure 4) were performed at very low C-rates (i.e., C/37 rate; ca. 10 mA g^{-1}). The first galvanostatic cycle, in which the solid electrolyte interphase layer is formed, is not shown. The second galvanostatic cycle shows that the closer the working elec-

 © 2009 Wiley-VCH Verlag GmbH & Co. KGaA, Weinheim

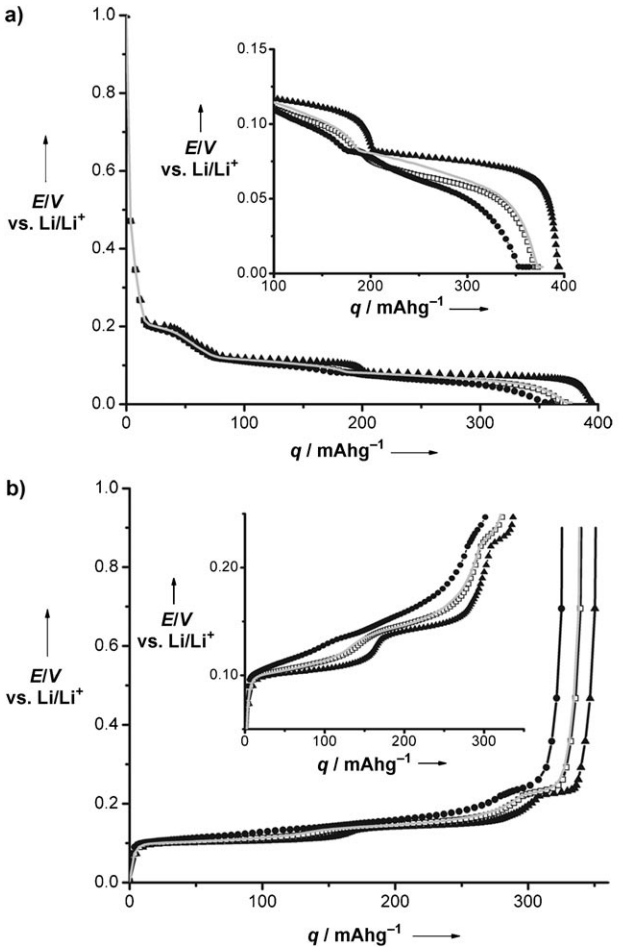

Figure 4. Galvanostatic plots of the MWE cell in the second electrochemical cycle during a) reduction and b) oxidation. Cycling took place between 1.000 and 0.005 V vs. Li/Li^+ at 10 $mA\,g^{-1}$. E = potential, q = specific charge. ▲ = WE1, □ = WE2, ● = WE3, solid gray line = sum of the contributions from each WE weighted by their mass fraction.

trode (WE1) is to the counter electrode (CE), the higher the specific charge. In addition, the redox plateaus are more pronounced if the working electrode is closer to the CE, which is due to a lower overpotential of the electrode.

A summary of the quantitative values obtained in this galvanostatic cycling is shown in Table 1. Note that each parameter is calculated based on the mass fraction of each layer of the WEs. During the reduction process (lithium insertion) in the second cycle, the specific charge differences between the WEs compared to the total applied charge were +4.6%, −1.1%, and −3.5% for WE1, WE2, and WE3, respectively. It should be noted that the current density distribution is not constant with time. The average current density distribution is linearly proportional to the integral of the current density over the specific period of time. Therefore, differences in specific charge are linearly proportional to the differences in the average current density. Interestingly, even at the low C-rate cycling of the MWE cell, we could still observe an inhomogeneity in the average current density distribution of more than 8% (Table 1).

Table 1: Electrochemical data for SFG44 graphite negative electrodes cycled between 1.000 and 0.005 V vs. Li/Li^+ at 10 $mA\,g^{-1}$.

Cell	q_{Red}[a] [$mAh\,g^{-1}$]	q_{Ox}[b] [$mAh\,g^{-1}$]	q_{BE}[c] [$mAh\,g^{-1}$]	q_{AE}[d] [$mAh\,g^{-1}$]	Δq_E[e] [$mAh\,g^{-1}$]
WE1	395.2	350.9	348.1	342.2	−5.9
WE2	373.5	339.9	283.1	281.6	−1.5
WE3	364.3	325.5	259.1	266.6	7.5
Total	377.7	338.6	296.8	297.0	0.2

[a] Specific charge of the second electrochemical cycle reduction process. [b] Specific charge of the second electrochemical cycle oxidation process. [c] Specific charge before the equilibration process under open-circuit conditions. [d] Specific charge after the equilibration process for 15 h under open-circuit conditions. [e] Difference between the specific charges during the equilibration process under open-circuit conditions. The cell was charged (lithium insertion) until the total specific charge reached 297 $mAh\,g^{-1}$ (equivalent to 80% SOC) before the equilibration process was started.

Furthermore, if the cell was cycled for 5 cycles and then stopped at 80% state of charge (SOC), at approximately 297 $mAh\,g^{-1}$ (based on the total active mass), the specific charge differences between the WEs compared to the total charge applied were even higher: approximately +17.3%, −4.6%, and −12.7% for WE1, WE2, and WE3. However, if the cell was left to equilibrate under open-circuit conditions for 15 h, the specific charge differences changed slightly to values of +15.2%, −5.2%, and −10.2% for WE1, WE2, and WE3. This implies that even an equilibration process of more than 15 h is not sufficient to solve this inhomogeneity challenge in the specific current distribution (Table 1).

We have recently demonstrated the possibility to estimate the SOC of a graphite negative electrode using an in situ colorimetry technique.[20] This technique is based on the fact that the graphite negative electrode has different colors at different levels of lithiation; golden-yellow regions are lithium-rich, whereas dark regions are lithium-deficient. After the MWE cell was left for equilibration under open-circuit conditions for 15 h at 80% SOC, the cell was disassembled to determine the color difference in each WEs (see Figure 5). In addition to the demonstration of lateral inhomogeneities,[20] the analysis of the yellowish/dark color regions provide an additional proof of the non-uniformity in the current density distribution between the WEs. We also observed some differences in color distribution between the top and the bottom sides of the WEs, which confirm that the inhomogeneity is perpendicular to the current collector.

In summary, we have shown herein that the MWE electrochemical cell is a unique tool for the quantitative study of current density distribution in a lithium-ion battery.

Experimental Section

TIMREX SFG44 synthetic graphite (TIMCAL SA, Switzerland) was applied as the electroactive material. The graphite negative electrodes were prepared by doctor-blading slurries of graphite active material (90 wt%) and poly(vinylidene fluoride) binder (10 wt%, SOLEF 1015, Solvay SA) in a *N*-methylpyrrolidinone (NMP) solvent onto a non-adhesive paper, from which the electrode mass was easily removed once dried. The electrodes were dried overnight using a vacuum oven at 120°C. After drying, these free-standing electrodes

 © 2009 Wiley-VCH Verlag GmbH & Co. KGaA, Weinheim

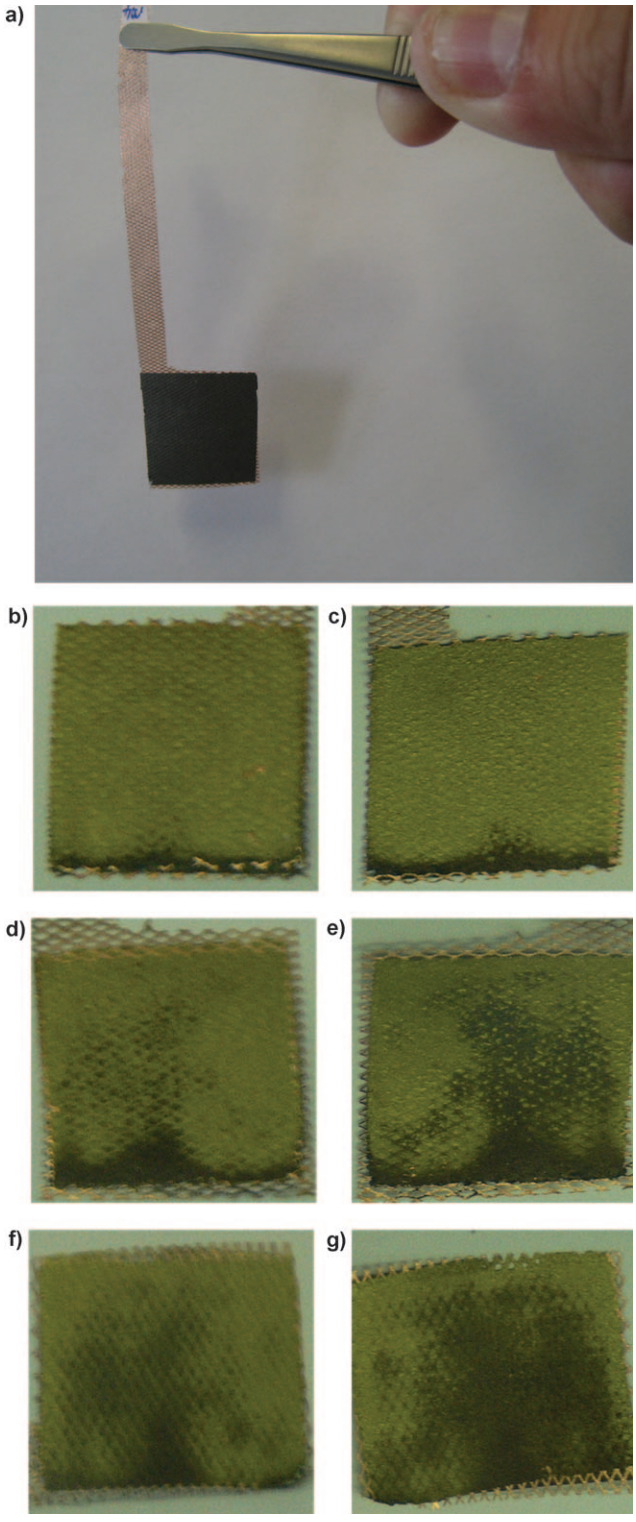

Figure 5. a) A photo of a WE (2×2 cm^2) before electrochemical cycling. b), d), and f) The top-side view (facing the CE); c), e), and g) correspond to the bottom-side view of lithiated graphite WEs for WE1, WE2, and WE3, respectively. The cell was charged (lithium insertion) until the total specific charge reached 297 $mAh\,g^{-1}$ (equivalent to 80% SOC) and left for equilibration under open-circuit conditions for 15 h, and finally disassembled in the glove box. The bright-yellowish regions are lithium-rich, whereas the darker regions are lithium-deficient sites.

(2 cm x 2 cm) were removed from the non-adhesive paper and subsequently pressed onto the respective current collectors (expanded copper mesh, circa 50 μm thick). The mass loading of each WE was typically 3–4 mg of active material per cm^2.

"Coffee bag"-type composite foil[21–23] was used as the host/body for the MWE electrochemical cell assembly. The composite foil consisted of four layers (circa 167 μm in total thickness): from the inside to the outside; a) polyethylene (PE), b) aluminum, c) PE, and d) oriented polyamide (OPA). The PE layer is thermo-sealable, whereas the OPA layer is not, and thus the OPA is placed on the outside of the MWE electrochemical cells. The aluminum inner layer (circa 12 μm thick) is an excellent barrier to both the O_2 and H_2O impurities. All cell components were dried overnight in vacuum at 120 °C and transferred to an argon-filled glove box. Finally, in the glove box, the MWE electrochemical cells were assembled by precise layer-by-layer arrangement of the WEs (Figure 1). Each WE and the counter electrode (metallic lithium) are separated by a layer of polymeric separator (Celgard 2500) soaked with a standard battery electrolyte (1M $LiPF_6$ in EC:DMC (1:1), Ferro GmbH). The neatly arranged electrode stack was later vacuum-sealed in the "coffee bag"-type cell.

Galvanostatic measurements were performed at a specific current of 10 $mA\,g^{-1}$ (of graphite) to complete the formation of the solid electrolyte interphase (SEI) in the first electrochemical cycle. When a potential of 5 mV vs. Li/Li^+ was reached, the lithiation step was continued until the total specific current dropped below 5 $mA\,g^{-1}$. The delithiation step was performed at a constant specific current of 10 $mA\,g^{-1}$ until a cut-off potential of 1.0 V vs. Li/Li^+. All measurements were carried out at room temperature. In addition, the specific current for each WE was monitored using individual general-purpose potentiostats (Model 2049, AMEL Instruments, Italy; labeled as P1–P3 in Figure 3). All terms related to charge (lithium insertion) or discharge (lithium extraction) used herein are defined based on the standard lithium-ion battery full-cell configuration.

Received: August 12, 2008
Published online: December 15, 2008

Keywords: batteries · current density · electrochemistry · graphite · lithium

[1] M. Winter, J. O. Besenhard, M. E. Spahr, P. Novák, *Adv. Mater.* **1998**, *10*, 725–763.
[2] S.-H. Ng, J. Wang, D. Wexler, K. Konstantinov, Z.-P. Guo, H.-K. Liu, *Angew. Chem.* **2006**, *118*, 7050–7053; *Angew. Chem. Int. Ed.* **2006**, *45*, 6896–6899.
[3] M. Armand, J.-M. Tarascon, *Nature* **2008**, *451*, 652–657.
[4] A. S. Aricò, P. Bruce, B. Scrosati, J.-M. Tarascon, W. Van Schalkwijk, *Nat. Mater.* **2005**, *4*, 366–377.
[5] P. G. Bruce, B. Scrosati, J.-M. Tarascon, *Angew. Chem.* **2008**, *120*, 2972–2989; *Angew. Chem. Int. Ed.* **2008**, *47*, 2930–2946.
[6] H. Buqa, D. Goers, M. Holzapfel, M. E. Spahr, P. Novák, *J. Electrochem. Soc.* **2005**, *152*, A474–A481.
[7] G. Ning, B. Haran, B. N. Popov, *J. Power Sources* **2003**, *117*, 160–169.
[8] V. S. Daniel-Bekh, *Zh. Fiz. Khim. SSR* **1948**, *22*, 697–710.
[9] J. Euler, W. Nonnenmacher, *Electrochim. Acta* **1960**, *2*, 268–286.
[10] J. S. Newman, C. W. Tobias, *J. Electrochem. Soc.* **1962**, *109*, 1183–1191.
[11] R. de Levie, *Electrochim. Acta* **1963**, *8*, 751–780.
[12] R. de Levie, *Electrochim. Acta* **1964**, *9*, 1231–1245.
[13] R. de Levie, *Electrochim. Acta* **1965**, *10*, 113–130.
[14] T. F. Fuller, M. Doyle, J. Newman, *J. Electrochem. Soc.* **1994**, *141*, 1–10.
[15] G. G. Botte, V. R. Subramanian, R. E. White, *Electrochim. Acta* **2000**, *45*, 2595–2609.

 © 2009 Wiley-VCH Verlag GmbH & Co. KGaA, Weinheim

[16] K. H. Kwon, C. B. Shin, T. H. Kang, C. S. Kim, *J. Power Sources* **2006**, *163*, 151 – 157.
[17] K. A. Smith, C. D. Rahn, C.-Y. Wang, *Energy Convers. Manage.* **2007**, *48*, 2565 – 2578.
[18] V. R. Subramanian, V. Boovaragavan, V. D. Diwakar, *Electrochem. Solid-State Lett.* **2007**, *10*, A255 – A260.
[19] http://en.wikipedia.org/wiki/Buffer_amplifier.
[20] P. Maire, A. Evans, H. Kaiser, W. Scheifele, P. Novák, *J. Electrochem. Soc.* **2008**, *155*, A862 – A865.
[21] T. Gustafsson, J. O. Thomas, R. Koksbang, G. C. Farrington, *Electrochim. Acta* **1992**, *37*, 1639 – 1643.
[22] J. M. Tarascon, A. S. Gozdz, C. Schmutz, F. Shokoohi, P. C. Warren, *Solid State Ionics* **1996**, *86–88*, 49 – 54.
[23] F. Rosciano, M. Holzapfel, H. Kaiser, W. Scheifele, P. Ruch, M. Hahn, R. Kötz, P. Novák, *J. Synchrotron Radiat.* **2007**, *14*, 487 – 491.

 © 2009 Wiley-VCH Verlag GmbH & Co. KGaA, Weinheim